Materials Science and Engineering B 271 (2021) 115258

Contents lists available at ScienceDirect

Materials Science & Engineering B

journal homepage: www.elsevier.com/locate/mseb

Spin waves excitation at micron-sized, anisotropy modified regions in amorphous $Fe_{80}B_{20}$ stripes: Local properties and inter-regions coupling

Unai Urdiroz [a], Cai Müller [b], Alicia Gómez [c], M. Teresa Magaz [c], Daniel Granados [d], Marta Sánchez Agudo [e], Juan Rubio-Zuazo [a,f], Germán R. Castro [a,f], Camelia Stan [g], Nobumichi Tamura [g], Howard A. Padmore [g], Federico Cebollada [e], F. Javier Palomares [a], Jeffrey McCord [b], Jesús M. González [b,*]

[a] Instituto de Ciencia de Materiales de Madrid (ICMM), A.E. Consejo Superior de Investigaciones Científicas (CSIC), 28049 Madrid, Spain
[b] Institute of Materials Science-Kiel University, Kiel 24143, Germany
[c] Centro de Astrobiología (CSIC-INTA), 28850 Torrejón de Ardoz, Spain
[d] IMDEA-Nanociencia, 28049 Madrid, Spain
[e] POEMMA-CEMDATIC, Escuela Técnica Superior de Ingenieros de Telecomunicación-Universidad Politécnica de Madrid, 28040 Madrid, Spain
[f] Spanish CRG BM25-SpLine Beamline at the ESRF, F-38043 Grenoble Cedex 09, France
[g] Advanced Light Source-Lawrence Berkeley National Laboratory, Berkeley, CA 94720, USA

ARTICLE INFO

Keywords:
Amorphous $Fe_{80}B_{20}$
X-ray irradiation
Anisotropy induction
Domain wall stabilization
Spin waves
Dispersion relationship
Group velocity
Phase velocity
Propagation distance
Decay time
Phase-shift

ABSTRACT

We report on the measurement of the local magnetization dynamics occurring, at units of GHz, in large aspect ratio stripes lithographed from reduced damping amorphous $Fe_{80}B_{20}$ films. The stripes were submitted to local anisotropy modifications by micrometric beam synchrotron X-ray irradiation. Our results include data on the dispersion relationships and group velocities corresponding to spin waves excited at both the non-irradiated and the irradiated regions. Whereas in the former case we observed standing spin waves with transverse-to-the stripe axis wave vector, in the latter one, for which the wave vector of the spin waves was parallel-to-the stripe axis, propagating spin waves were excited. In both regions, we measured the effective propagation distance of the spin waves, which resulted to be independent of the wave vector orientation. In the spin waves excited at the irradiated region, we also measured the decay time and effective damping coefficient, which was in good agreement with previously reported values obtained from FMR measurements in amorphous $Fe_{80}B_{20}$ continuous films. We show that the interaction of the non-irradiated and irradiated zones results, at the stripe transverse saturation remanence and under an exciting field frequency of 4 GHz, in the introduction of a π phase shift between the standing spin waves excited at both sides of the irradiated region. This result opens the possibility of using the local, transverse to the stripe axis, magnetic anisotropy easy axis induced by the X-ray irradiation as a crucial constituent of a zero-applied field spin wave phase-shifter.

1. Introduction

Spin waves are collective excitations of magnetically ordered systems that were first introduced in the context of the decrease of the spontaneous ferromagnetic magnetization with the increase of the temperature [1,2], where they provided a successful framework to account for the experimental observations in a broad range of materials [3]. Spin waves, and their short wavelength, quasi-particle quantum equivalent, the magnons are the first excited states of Hamiltonians incorporating exchange and/or dipolar interactions, and whose relative weight determine the spin waves wave vector magnitude. Spin waves have been characteristically investigated resorting to inelastic neutron [4], light [5], and electron scatterings [6] and to ferromagnetic resonance [7]. All three scattering techniques, having different sample mass requirements and energy resolution characteristics, are based on the measurement of the particles incident beam energy loss associated to the

Abbreviations: NIS, Non-Irradiated Stripe; IR, Irradiated Region; AM, Anisotropy modified region.

* Corresponding author at: Departamento de Nanoestructuras y Superficies, Instituto de Ciencia de Materiales de Madrid – CSIC, c/ Sor Juana Inés de la Cruz 3, 28040 Madrid, Spain.
E-mail address: jm.g@csic.es (J.M. González).

https://doi.org/10.1016/j.mseb.2021.115258
Received 11 November 2020; Received in revised form 5 May 2021; Accepted 19 May 2021
Available online 22 June 2021

excitation of spin waves and allow obtaining the spin waves dispersion relationships. Differently, the microwaves absorption based, ferromagnetic resonance is specifically used to investigate the links between the magnetic anisotropy and the spin waves dispersive properties [8,9].

On the basis of the experimental and theoretical fundamental spin waves studies initiated in the early 50′s [2], the last two decades have witnessed a very relevant intensification of the interest on the study of the spin waves from the standpoint of their practical uses. In a large majority of cases, this involved the exploitation of the undulatory nature of the spin waves (this research field is called spin waves optics or, more usually, magnonics). In fact, application focused research activities have prompted the emergence of a large deal of plausible technological uses, that, very relevantly, included both information processing devices and their associated circuitry [10] (i.e.: spin waves guides).

This research scenario has been fueled by the simultaneous progress on i) the availability of high-quality oxide and metallic films, adequate to get nanostructured by using conventional technologies [11], ii) the development of new experimental techniques to follow the response of the magnetization to high frequency magnetic fields (up to THz) [12–14], and iii) the conceptual proposal of a comprehensive range of new, spin waves-based, circuitry and devices [15] potentially able of being exploited in functionally complete information transport and processing nano-systems. The main advantage of the magnonic process devices, with respect to the conventional semiconductor technologies, is related to the fact that the spin waves propagation do not involve charge transport and henceforth are almost free from heat dissipation problems. Likewise, in the context of the currently available 10 nm (Tri-Gate) semiconductor technologies, the identified disadvantages of the spin waves use (i.e.: their slow group velocity and large attenuation, if compared with electromagnetic radiation) are, due to the reduced device design length scales, no longer relevant and some specific spin waves properties as i) easy integration with guides, ii) inductive transduction, and iii) very flexible properties tuning implementable by applying magnetic fields [13–14] become high value assets both from the implementation and the new device design viewpoints. Considering all of these aspects, the spin waves related phenomenologies and technologies constitute a research field gathering an increasingly large amount of interest, resources and efforts [10,16–17]. In particular, and focusing on the advances on the design of processing devices, the recent developments mostly correspond to the logic gate family [15]. Different logic gates functionalities have been implemented on the basis of interferometric designs [18] (e.g.: NOT gate, XNAND gate, etc.). In all the cases, spin waves phase shift keying (PSK) coding was used in order to represent the binary symbols (i.e.: the “0″ and “1” symbols are associated to spin waves of the same frequency and whose phases differ in π). From this, it is clear the relevance of controlling the spin waves phase and, more concretely, that of generating spin waves, in-guide π phase shifts. Dobrovolskiy et al, have recently shown how engraving a nanoscale trench in a micron wide spin waves guide, by means of a focused ion beam, allows to continuously vary, for a given trench depth, the phase of spin waves propagating across the nanotrench by varying the dc bias field [19]. A simpler phase-shifter was proposed by Hertel et al. [20] who considered the presence of a wall transversally stabilized in a spin waves guide. Their dynamics simulations allowed to evidence the functionality of the wall as a π phase shifter under zero dc applied field, but, up to date, no practical implementation of this design principle has been demonstrated due to the difficulties related to the stabilization in a spin wave guide of a wall with the required characteristics.

Our work focuses on the measurement of the properties of the spin waves excited in stripes (lithographed from amorphous, reduced damping [21] $Fe_{80}B_{20}$ films) in which we have induced, by means of synchrotron X-rays irradiation, a micrometric-sized region having modified local anisotropy compatible with the stabilization of a 180° wall [21]. By means of time resolved magneto-optic Kerr effect, we have quantified the local dynamic properties (dispersion relationship, group and phase velocities, and propagation distance) of standing (non-irradiated region) and propagating (irradiated, anisotropy modified region) spin waves as well as, in the propagating spin waves case, measured their decay time and effective damping coefficient. We have also examined the interactions, regarding the spin waves excitation, between the irradiated and non-irradiated zones to conclude that a π phase shift between standing waves excited at both sides of the irradiated region occurs at zero bias dc field (once the stripe is prepared at its transverse to the stripe long axis dc saturation remanence).

2. Samples and experimental

Films having a nominal $Fe_{80}B_{20}$ atomic percentage composition, were deposited, with a thickness of 15 nm, by using a pulsed laser ablation deposition (PLAD) system, working under ultrahigh vacuum conditions, from polycrystalline targets with the same composition than the films and onto Corning® glass substrates. The composition of the deposits was measured by means of X-ray photoelectron spectroscopy (XPS). X-ray diffractograms were taken from the as-deposited films in order to check their amorphicity. The diffraction measurements were taken at the ESRF (Beamline BM25-B Single Crystal Diffraction Branch) by using a monochromatic beam with an energy of 20 keV.

We prepared, from the as-deposited films and by using maskless laser lithography, arrays of large aspect ratio stripes having 750 μm length, and either 15 μm (SA samples) or 25 μm (SB samples) widths and sufficiently distant so as not to be magnetically interacting. X-ray irradiation treatments were performed onto the lithographed stripes at the Advanced Light Source (ALS) at Microdiffraction Beamline 12.3.2, by means of a ”pink-beam” with energies in the range from 6 keV up to 24 keV, a spot of 2 μm × 28 μm, an incident photons flux of 8.5×10^{10} photons/s [22], an incidence angle over the sample of 3°, and irradiation times of 10 s (SA10 sample), 30 s (SA30 sample) and 15 s (SB15 sample). In order to position the stripes with respect to the X-ray beam before irradiations (in all cases the irradiated region center coincided with the stripe center), fluorescence mapping, measured at the Fe-K absorption edge by exposure to a 10 keV monochromatic beam was used. The occurrence of crystallization during the irradiation process was checked by X-ray diffraction (XRD) measurements performed, at the energy used in the fluorescence mapping by resorting to a two-dimensional detector, before and after each irradiation run.

The dc and dynamic magnetic responses of the stripes were quantitatively imaged by means of quasi-static and time-resolved stroboscopic wide-field magneto-optic Kerr effect (MOKE) microscopy [23–25] with oblique incidence and s polarized light (electric field oriented perpendicularly to the plane of incidence). For that configuration, the experiments yield a mixed signal, comprising both a longitudinal Kerr effect contribution, giving the in-plane magnetization component parallel to the incidence plane, and a polar Kerr effect one, which measures the out-of-plane magnetization component. The MOKE contrast shown in all the Figures corresponds mainly to the longitudinal Kerr effect, due to the large in-plane magnetization component resulting from the reduced thickness of our samples (the only exception to this is Fig. 19 that will be specifically discussed later). Time-resolved MOKE (TRMOKE) images were acquired by simultaneously submitting the samples to a sinusoidal excitation magnetic field H_{rf} (with frequencies from 1 GHz up to 8 GHz and, in all the measurements, a base-to-peak field amplitude of 3.8 Oe) and to a (perpendicular to H_{rf}) quasi-static magnetic field H_{dc} having a maximum magnitude of 250 Oe. Measurements were performed by placing the sample upside down on a coplanar wave-guide creating the H_{rf} field. TRMOKE images were acquired at different time delays with respect to an imaging trigger (the delays ranged from 0 to 9/8 of the H_{rf} period with a time increment step of 1/8 of that period) and, in all the cases, were subtracted from a reference image further delayed by one half of the period. Dc magnetization loops were measured by recording the MOKE intensity per pixel during the magnetization reversal induced by quasi-static H_{dc} field cyclic variations (performed while keeping $H_{rf} = 0$).

3. Results and discussion

XPS spectra taken on the as-deposited films evidenced that their composition was that of the PLAD targets, i.e.: $Fe_{80}B_{20}$ in atomic percentage. The as-prepared films, were X-ray diffraction amorphous down to the resolution of the technique. Samples isothermally treated for 60 min in high vacuum and above 250 °C exhibited XRD partial crystallization, whereas those annealed above 350 °C where fully polycrystalline and isotropic [21].

The as-deposited films displayed uniaxial magnetic anisotropy (as evidenced from the measurement of the in-plane angular dependencies of the hysteresis and the ferromagnetic resonance) [26–27] with an anisotropy constant $K_o = 1.0 \times 10^4$ erg/cm^3 (measured as all the other anisotropy constant values in the manuscript, by considering the hard axis expression $K_o = (1/2)\, M_S\, H_{Kha}$, from the magnetometric value of the films saturation magnetization, $M_S = 14400$ G [26], and the measured hard axis saturation field, $H_K = 17$ Oe). Upon a relaxation heat treatment (60 min at 165 °C) the anisotropy constant decreased down to $K_{ann} = 0.6 \times 10^4$ erg/cm^3. In Fig. 1 we have plotted the in-plane, MOKE dc field hysteresis loops measured in a non-irradiated stripe (NIS) by applying the field along and across the stripe long symmetry axis (those fields orientations will be named, in the following, longitudinal axis field and transverse axis field, respectively). The longitudinal axis loop showed close-to-perfect square behavior, whereas the transverse axis loop was almost anhysteretic, with close-to-zero remanence and a saturation field of the order of 35 Oe. From these loops we conclude that the shape of the NIS (having large aspect ratio and reduced thickness: 750 μm × 15 μm × 15 nm) originated an effective easy axis parallel to the stripe long symmetry axis having a measured anisotropy constant of $K_{NIS} = 2.1 \times 10^4$ erg/cm^3 (measured from the hard axis saturation field).

In all the samples the XRD patterns taken after the irradiation allowed us to exclude, down to the resolution of the technique, the local presence of crystallites at the irradiated region (IR). The effects of the irradiation on the magnetic behavior of the stripes can be identified on the magnetic domain structure occurring at and near the IR. Fig. 2 shows the domain structure, imaged by MOKE, and present at the stripe saturation remanences corresponding to longitudinal, Fig. 2 a), and transverse, Fig. 2 c), in-plane applied dc fields (in Fig. 2 a) and 2c), taken in sample SA10, the measured magnetization components are longitudinal and transverse, respectively). In the longitudinal field remanence case, it is possible to observe contrast at the IR, corresponding to two differently oriented domains, and between the IR and the non-irradiated areas. In the case of the image corresponding to the transverse field remanence, Fig. 2 b), it is apparent the occurrence, within and near the IR, of two

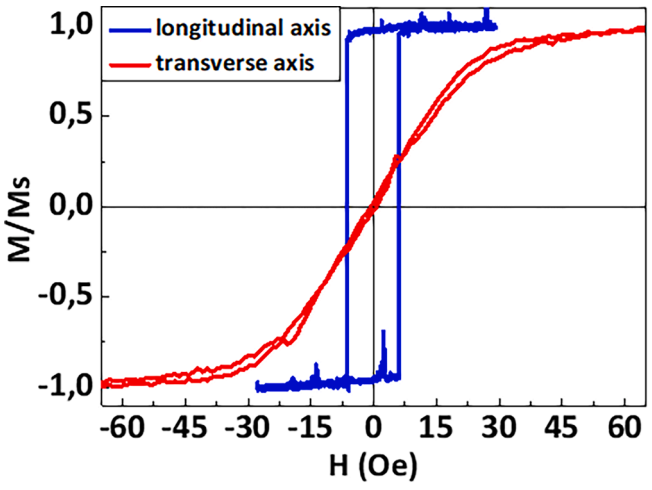

Fig. 1. Dc in-plane hysteresis loops measured along the NIS longitudinal and transverse axes.

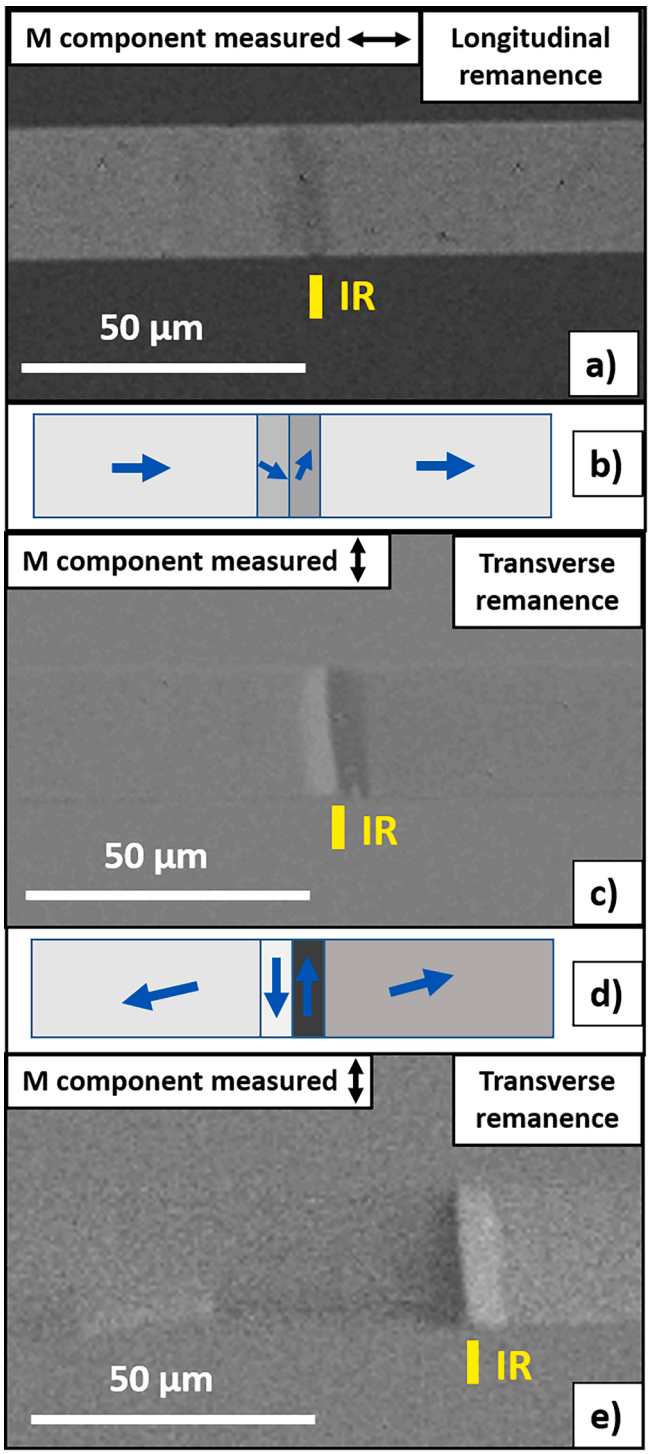

Fig. 2. Magnetic domains structures imaged around the IR in SA10 sample upon taking the stripe to its a) longitudinal, and c) and transverse saturation remanences. Diagrams b) and d) illustrate the measured average directions of the local magnetization corresponding to the a) and b) images, respectively. Image e) shows the domain structure near the IR at the transverse remanence of SA30 sample and, particularly, the occurrence of asymmetric structures including domain walls parallel to the stripe axis.

antiparallel magnetic domains. Those domains are separated by a 180° wall and associated to magnetization pointing close-to-transversely to the stripe axis. In the diagrams in Fig. 2 b) and 2 d), the arrows show the MOKE measured directions of the magnetization at the 2 a) and 2c) images, respectively. From Fig. 2 we conclude about the presence at and

near the IR of a local anisotropy modification associated to the induction of a transverse local easy axis. In a recent paper [21] the authors have analyzed in detail the local anisotropy distribution induced by the irradiation (in SA and SB samples) at the anisotropy modified (AM) zone. That anisotropy modification, linked to a local easy axis direction independent of the irradiation time and the stripe width [22], was identified as the result of the moderate local heating produced by the X-ray and the stress fields experienced by the IR and resulting from its elastic coupling to the substrate and/or the non-irradiated stripe region. From the measurement of the local hysteretic properties, it was concluded [22] that the transverse easy axis region had an approximate width of 6 μm, and that, at both sides of that region, transition zones where the anisotropy easy axis evolved from the transverse direction to the longitudinal one (associated to the non-irradiated zone) happened. The total dimension along the stripe axis of the AM zone was estimated in 16 μm (i.e.: each one of the transition zones had a length of ca. 5 μm). Fig. 2 e) shows the local magnetic domains observed in sample SA30 at the transverse remanence and near the IR that are a direct consequence of the described anisotropy modified zone characteristics and of the magnetostatic energy minimization. The observed transverse domains (pinned in some samples for field ranges which are of the order of 20% of the coercivity) [21] include the presence of asymmetric structures, including walls parallel to the stripe axis and separating domains, presumably nucleated at the stripe edges from the central stripe magnetization.

Prior to any TRMOKE measurement, the sample was ac demagnetized, prepared according to the applicable procedure (e.g.: at a saturation remanence), and MOKE imaged at the intended measurement site. This was done in order to identify the characteristics of the local dc magnetization distribution and, particularly, to ascertain the presence of a 180° transverse wall at the IR like that seen in Fig. 2 (and also in the SA 30 and SB 15 samples [21]). Since that wall provides the basis for the observed dynamic phenomenology, we conclude that the results shown for sample SA 10 are general. Fig. 3 a) shows a TRMOKE snapshot obtained in SB15 sample far from the IR, at the stripe longitudinal field saturation remanence, and with the sample submitted to a transverse, 3 GHz, H_{rf} field. The measured contrast corresponds to the transverse magnetization component. Fig. 3 a) identifies lines 1 and 2 along which the data plotted in Fig. 3 b) and 3c) are measured, respectively. From these plots, showing the position dependencies of the instantaneous TRMOKE signals measured along the stripe longitudinal and transverse directions, respectively, we can conclude that the observed contrast corresponds to the occurrence of standing spin waves with a transverse wave vector (getting reflected at the stripe edges), and leading to a Damon-Eshbach geometry. The excitation of spin waves in this experiment is due to the nonuniform demagnetization fields at the edges of the stripes [28–29]. The standing nature of the observed spin waves is explicitly shown in Fig. 4, where we display TRMOKE images taken, at the longitudinal remanence, under a transverse H_{rf} field having a frequency of 3.5 GHz, and for different time delays with respect to the used image trigger signal (the bottom panel shows a sketch of the position dependencies across the stripe of the instantaneous TRMOKE signal corresponding to the different images shown). The occurrence of moment pinning at the stripe edges is explicitly shown in Fig. 5, where we present images of the stripe taken at different H_{rf} field frequencies, in the range from 2.5 GHz up to 4.0 GHz. Beside those images we have plotted the position dependencies of the local TRMOKE signal amplitudes measured across the stripe and associated to the different H_{rf} frequencies (the shown values correspond to averages of the local raw TRMOKE signal amplitudes obtained along 2 μm lines perpendicular to the wave vector and covering the stripe transverse direction). Those plots allow to identify the first three odd modes of the excited standing waves, and therefore to measure the excited spin waves wavelengths. Higher order modes are not observable as a consequence of the decrease of the TRMOKE signal amplitude, which becomes comparable to the experimental set-up noise level, with the increase of the mode order.

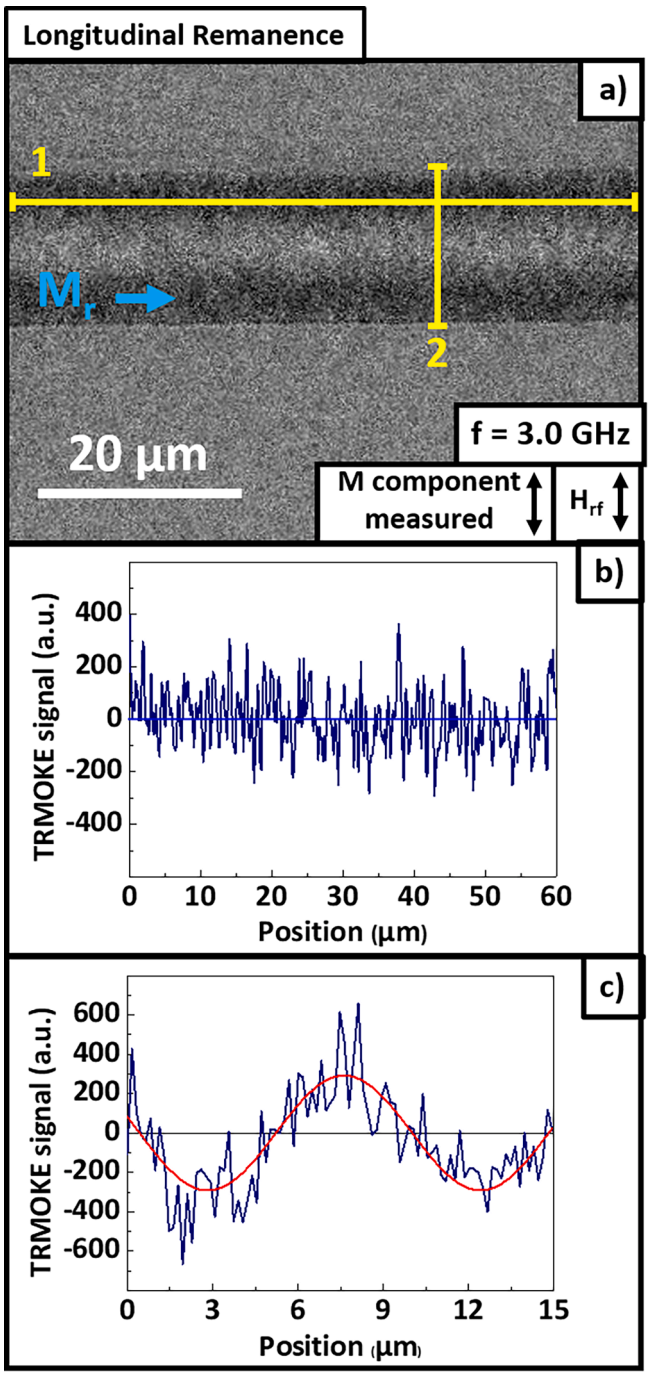

Fig. 3. a) TRMOKE image taken by applying the fields and implementing the measuring configurations indicated (the measured local dc remanent magnetization direction is shown with the blue arrow), b) Position dependence of the instantaneous TRMOKE signal measured along line 1 in a) (zero position corresponds to the most leftward point in line 1), and c) Position dependence of the instantaneous TRMOKE signal measured along line 2 in a) (zero position corresponds to the upper stripe edge).The red line corresponds to a sinusoidal data fit. (For interpretation of the references to colour in this figure legend, the reader is referred to the web version of this article.)

A dynamic behavior qualitatively similar to that observed at the longitudinal remanence can be seen when the stripe is simultaneously submitted to a transverse H_{rf} field and a saturating dc longitudinal field. Fig. 6 shows the modes observed in the SB15 sample for a longitudinal field $H_{dc} = 250$ Oe and transverse H_{rf} fields having frequencies in the range from 6.5 GHz up to 7.5 GHz. The dependencies on the position

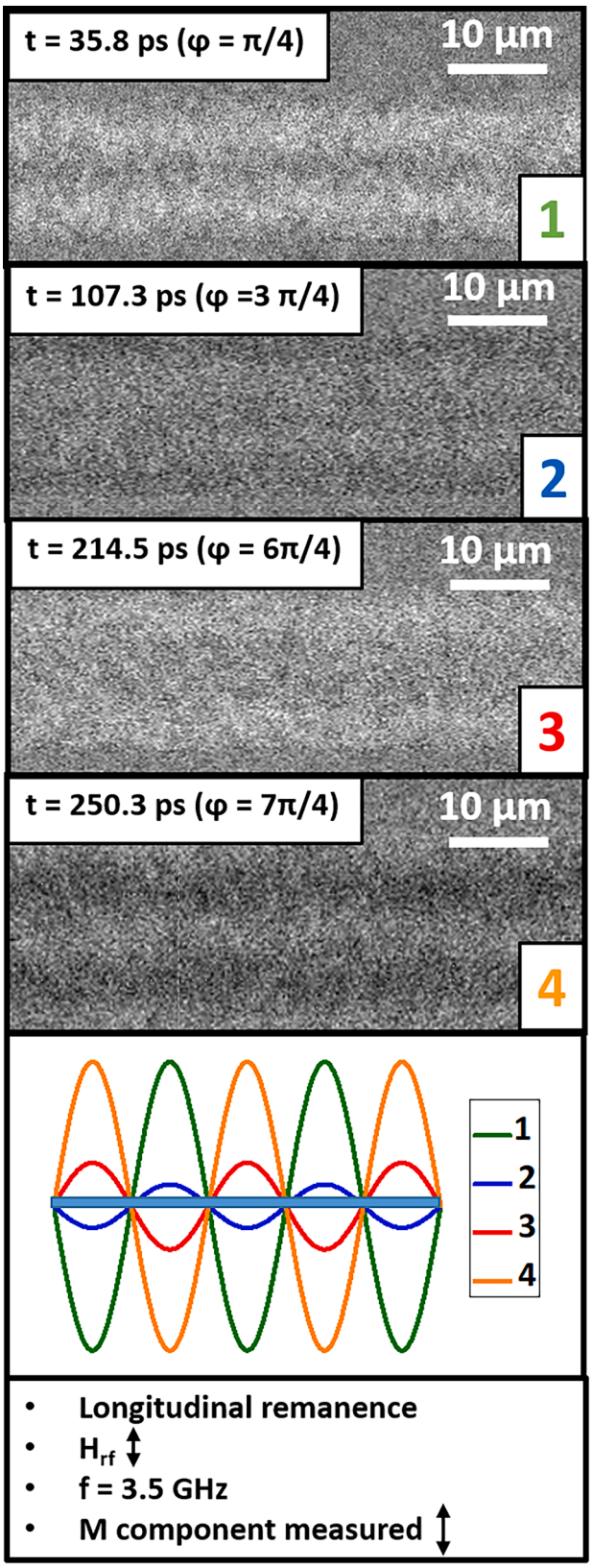

Fig. 4. TRMOKE images obtained, far from the IR, at the stripe longitudinal remanence and under a transverse H_{rf} field having a frequency of 3.5 GHz. The images correspond to different time delays with respect to an arbitrary imaging trigger signal (the associated phases are also indicated). The bottom center panel shows a sketch of the instantaneous TRMOKE signal measured transversally to the stripe axis.

across the stripe of the local TRMOKE signal amplitude allow, in this case, to identify the n = 3, n = 5, and n = 9 modes. The highest mode data evidence a clear decrease of the standing spin waves amplitude with the decrease of the distance to the stripe center that is associated to an amplitude minimum at that region. The fit, for n = 9, of the experimental data to two sinusoids, with amplitudes exponentially decreasing from both stripe edges, yields a propagation distance (associated to an amplitude decrease of 90% from the values measured near the edges) of 17 μm.

The standing spin waves modes identification shown in Fig. 6, allows us to directly evaluate their wave vectors (from the measurement of the standing waves wavelength) at the different H_{rf} field frequencies. Thus, it is possible to collect information on the dispersion relationship associated to the excitation of spin waves at the non-irradiated region. Fig. 7 presents (full symbols) our data for the transverse, standing spin waves observed at the longitudinal saturation remanence and upon application of a longitudinal field H_{dc} = 250 Oe. We have fitted our experimental data to the a) dipole–dipole model [30], without getting an acceptable description of the measured data and b) the dipole-exchange spin waves dispersion relationship proposed by Tacchi [31] given by

$$\omega_k^2 = \left\{\omega_H + \omega_M\delta\left[k^2 + \left(\frac{\pi}{L}\right)^2\right] + \omega_M\left[1 - \left(\frac{kL}{\pi}\right)^2\right] - \omega_U\right\}\left\{\omega_H + \omega_M\delta\left[k^2 + \left(\frac{\pi}{L}\right)^2\right] + \omega_M\left(\frac{kL}{\pi}\right)^2\right\} \quad (1)$$

where ω_K is the spin waves angular frequency, $\gamma/2\pi$ = 28.02 GHz/T is the electron gyromagnetic ratio [32] $\omega_H = \gamma H_{dc}$ gives the frequency equivalent of the H_{dc} applied field; $\omega_M = \gamma 4\pi Ms$ = 253.5 GHz gives the frequency equivalent of the saturation magnetization (Ms = 14400 G [26]); $\omega_U = \gamma 2k_U/Ms$ gives the frequency equivalent of the effective anisotropy, $\delta = l^2_{ex} = A_{ex}/2\pi M_S^2$ is the square of the exchange correlation length (given by the ratio of the exchange constant, A_{ex}, to the dipolar energy density $2\pi M_S^2$; L is the film thickness and k is the spin waves wave vector. Our best fit results are represented in continuous lines in Fig. 7. In particular, we considered as fitting parameters the stripe thickness, L, and the value of the square of the exchange correlation length, δ. The obtained squared exchange correlation length values, are $\delta = 1.9 \times 10^{-13}$ cm^2 for the longitudinal remanence and $\delta = 1.5 \times 10^{-13}$ cm^2 for the H_{dc} = 250 Oe case. Both of them are in good agreement with the value ($\delta = 1.1 \times 10^{-13}$ cm^2) obtained by considering Ms = 14400 G and $A_{ex} = 10^{-6}$ erg/cm which indicates the actual occurrence of an exchange contribution to the dispersion behavior of the transverse standing spin waves excited in the non-irradiated zone. Nevertheless, the agreement of our data with the Tacchi model is not complete since the stripe thicknesses coming out from the fits are L = 227 nm, for the longitudinal remanence, and L = 130 nm for the H_{dc} = 250 Oe field, both of them clearly above the nominal L value, L = 15 nm. We understand that disagreement as related (in addition to the reduced amount of data used for the fit) to the order of magnitude of the measured wave vectors, some units of rad/μm, in the conventional limit between the dipole-exchange region and the magnetostatic excitations region [34]. The inset in Fig. 7 shows the wave vector dependence of the group velocity evaluated (for both the longitudinal remanence and a longitudinal field H_{dc} = 250 Oe) from the fit of our experimental dispersion data to equation (1). Our results correspond to a maximum velocity of ca. 16 km/s for the remanence case and wave vectors above 2 μm^{-1}.

In the applied field H_{dc} = 250 Oe case velocities of up to ca. 5 km/s are obtained for wave vectors having a magnitude of 2.5 μm^{-1}. Fig. 8 displays our results for the evaluation of the dependence on the wave vector magnitude of the phase velocity obtained from the dispersion data. Those velocities range from 60 km/s, measured at the longitudinal remanence and a wave vector of 0.26 μm^{-1}, down to 20 km/s obtained for a dc field of 250 Oe and a wave vector of 2.81 μm^{-1}.

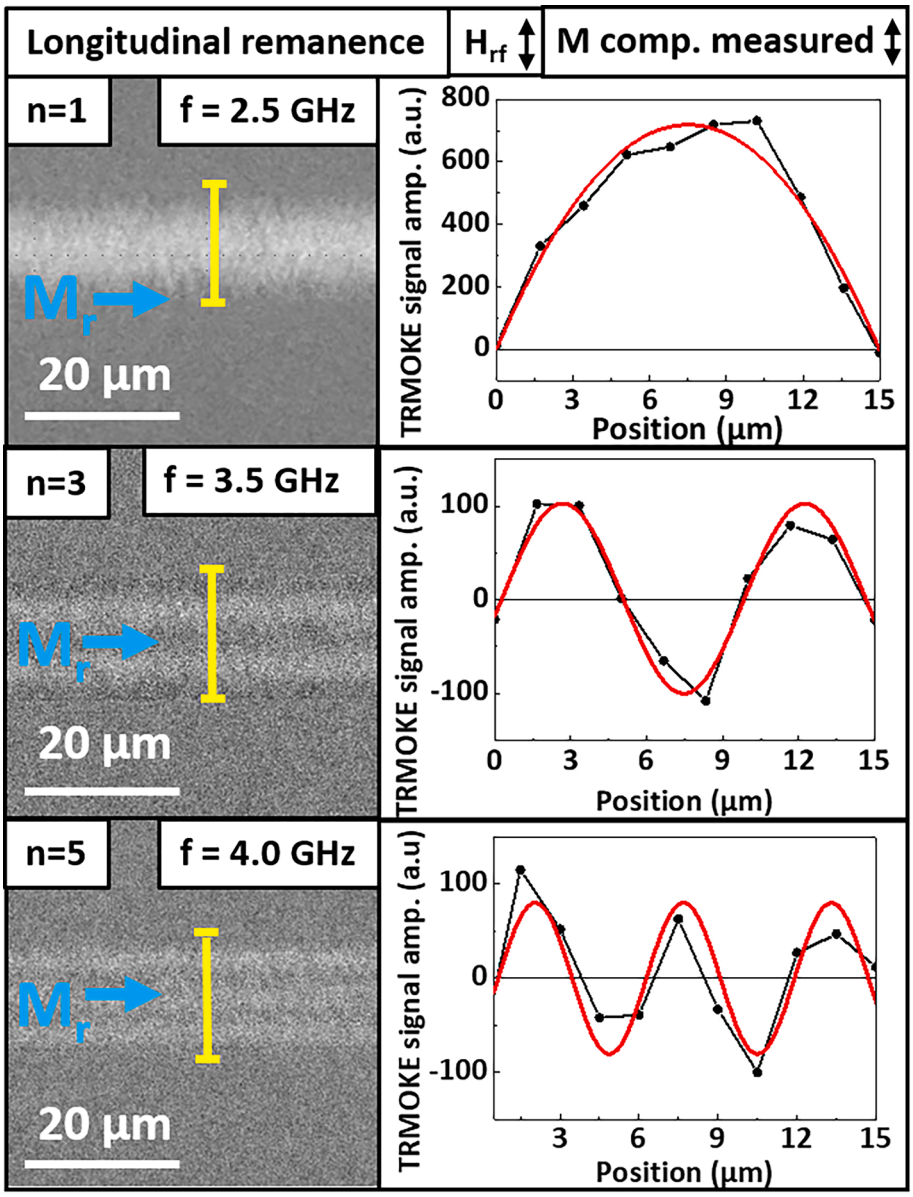

Fig. 5. TRMOKE images corresponding to the first three standing spin waves odd modes excited in the non-irradiated zone at the longitudinal remanence and under transverse H_{rf} fields having frequencies of 2.5 GHz, 3.5 GHz and 4.0 GHz (the measured local dc remanent magnetization direction is shown with the blue arrows). The plots beside each image show position dependencies of the local TRMOKE signal amplitude measured along the transverse lines indicated in the images (zero position corresponds to the upper stripe edge). The red lines in the plots correspond to the fits of the data to sinusoidal functions. (For interpretation of the references to colour in this figure legend, the reader is referred to the web version of this article.)

Considering now the dynamic behavior results obtained at the AM zone, let us recall that the local easy axis at the IR is oriented perpendicularly to the stripe long axis. Fig. 9 a) shows a TRMOKE image (taken in the SB15 sample) of the region around the AM zone obtained by submitting the stripe to a transverse dc field $H_{dc} = 40$ Oe and to a longitudinal H_{rf} field having a frequency of 4.0 GHz. The observed contrast corresponds to the longitudinal component of the magnetization. The image illustrates the excitation of spin waves in a region having a longitudinal dimension of the order of 20 μm. According to the instantaneous TRMOKE signal profiles shown in Fig. 9 b) and 9c), measured along the transverse (line 1 in Fig. 9 a)) and longitudinal (line 2 in Fig. 9 a)) directions, respectively, we conclude that the wave vector of these spin waves is oriented longitudinally.

The spin waves observed close to the IR are of the propagating type as it can be seen in Fig. 10 a) where we present the time evolution (measured after a zero time associated to an arbitrary imaging trigger) of the instantaneous TRMOKE signal recorded at a position range corresponding to distances from the center of the IR of up to 8 μm (transverse $H_{dc} = 40$ Oe, H_{rf} frequency of 4.0 GHz). The spatial displacement, across the mentioned region, of an individual maximum of the instantaneous TRMOKE signal is identified with blue arrows. That displacement corresponds to an approximate phase velocity of 22 km/s (Fig. 10 b)).

The propagating spin waves excited at the AM zone, as those imaged in Fig. 11 a), are emitted from the center of the IR (as expected considering the parallelism at that region of the local easy axis and the applied dc field). Their amplitude decreases with the increase of the distance to the emission point as it is shown in the plot in Fig. 11 b), corresponding to the spatial variation of the local TRMOKE signal amplitude at the AM zone. The plotted data correspond to points in a line parallel to the stripe axis near the lower edge of the imaged stripe. At other lines, parallel to the considered one but displaced from the stripe lower edge, the measured data are slightly different from those plotted here due to a detectable inhomogeneity across the stripe of the irradiation, originating different degrees of saturation at different positions across the stripe. The data correspond to spin waves excited by a longitudinal H_{rf} field with a frequency of 4.0 GHz under a transverse dc field, $H_{dc} = 40$ Oe. The results in Fig. 11 b) have been fitted (red line in Fig. 11 b)) to a sinusoid whose amplitude decays exponentially from the

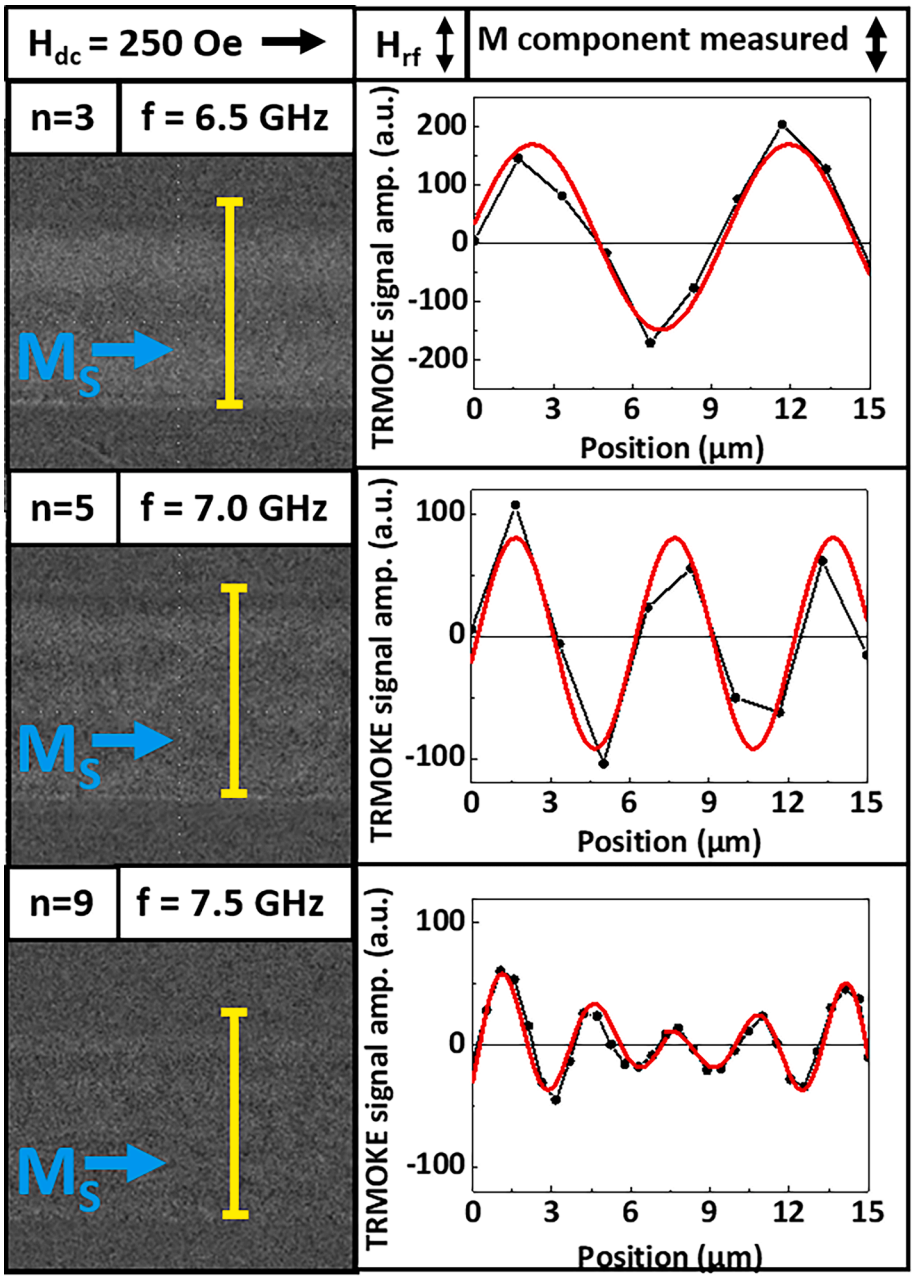

Fig. 6. TRMOKE images corresponding to the n = 3, n = 5 and n = 9 transverse standing spin waves modes excited upon application of a longitudinal saturating field H_{dc} = 250 Oe while keeping the sample under transverse H_{rf} fields having frequencies of 6.5 GHz, 7.0 GHz and 7.5 GHz, respectively (the measured local orientation of the dc magnetization direction is shown with the blue arrow). The plots beside each image, allowing to identify the modes order, show the position dependencies of the TRMOKE signal amplitudes measured along profiles (indicated in the snapshots) transverse to the stripe long axis (zero position corresponds to the upper stripe edge). The red lines in the plots corresponding to H_{rf} frequencies of 6.5 GHz and 7 GHz are fits of the data to sinusoidal functions with the field frequency. The red line in the 7.5 GHz plot corresponds to two sinusoids with the H_{rf} field frequency and having exponentially decaying (from both stripe edges) amplitudes. (For interpretation of the references to colour in this figure legend, the reader is referred to the web version of this article.)

center of the IR (green line in that Figure). Fig. 12 summarizes our results (full symbols) for the dispersion relationships verified by the longitudinal waves propagating from the AM zone under applied H_{dc} fields of 30, 40, and 150 Oe. Likewise, the standing transverse spin waves, these relationships have been fitted using equation (1) obtaining exchange correlation parameters significantly smaller than those obtained for the transverse spin waves: $\delta = 5.2 \times 10^{-14}$ cm^2 $\delta = 6.9 \times 10^{-14}$ cm^2 and $\delta = 1.0 \times 10^{-14}$ cm^2 for 30 Oe, 40 Oe, and 150 Oe, respectively. The values obtained for the stripe thickness are also larger than the nominal value (L = 79 nm, L = 110 nm, and L = 177 nm, for 30 Oe, 40 Oe, and 150 Oe, respectively). In addition to the points raised in the case of the standing transverse spin waves, the disagreement of our data with the Tacchi model could also correspond to the fact that the longitudinal waves propagate in an inhomogeneous anisotropy region including the IR, the transition region from the IR to the non-irradiated zone and even the non-irradiated zone (see Fig. 11 b)). That inhomogeneity of the anisotropy could be linked to the occurrence of larger magnetostatic (dipole–dipole) interactions than those occurring in the case of the standing transverse spin waves (being excited in a homogeneous anisotropy region) and also to the absence of spin pinning at the limits of the zone where the spin waves propagate (which allows for the existence of larger local magnetic pole densities at those limits). As it is clear from Fig. 12, in the lower applied dc field range the magnitude of that field only slightly influences the observed spin waves dispersion law. This is not the case when higher dc fields are applied. The inset in Fig. 12 shows our results for the wave vector dependence of the group velocity, obtained from the dispersion relationship data. The group velocity increases with the applied dc field value reaching values of ca. 11 km/s at H_{dc} = 150 Oe and wave vectors larger than 4 μm^{-1}. These values are in the order of magnitude corresponding to other materials currently considered for magnonic applications such as YIG (2.6 km/s) [34], Permalloy (18 km/s) [35], CoFeB (25 km/s) [36] or YIG-Pt bilayers (1

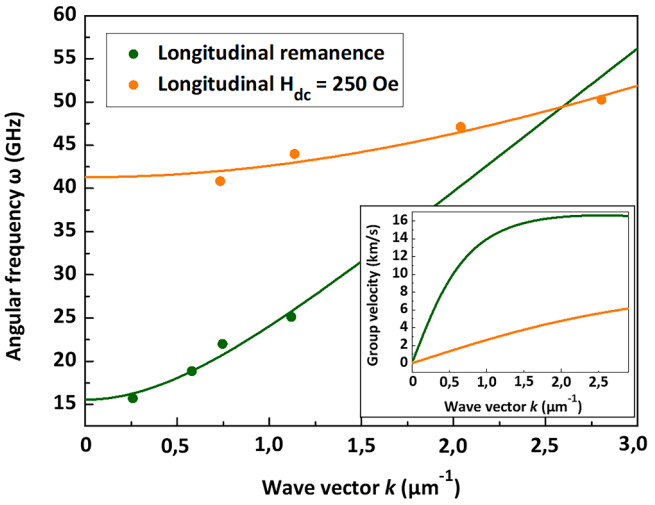

Fig. 7. Experimental dispersion relationships data (full symbols) corresponding to the longitudinal remanence (green circles) and a longitudinal applied field H_{dc} = 250 Oe (orange circles). The continuous lines in the main panel correspond to the fit of the experimental data to equation (1) with the parameters detailed in the text. The inset shows the wave vector dependence of the spin waves group velocity obtained from the fits of the dispersion relationships data (the green line corresponds to the longitudinal remanence and the orange one to a longitudinal applied field H_{dc} = 250 Oe). (For interpretation of the references to colour in this figure legend, the reader is referred to the web version of this article.)

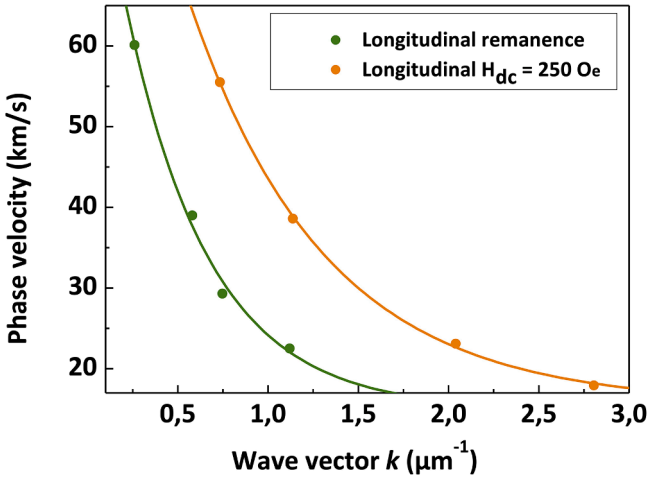

Fig. 8. Phase velocity (full symbols) variation with the transverse standing spin waves wave vector evaluated from the experimental dispersion relationships data corresponding to the longitudinal remanence (green circles) and to a longitudinal applied field H_{dc} = 250 Oe (orange circles). The continuous lines are guides for the eye. (For interpretation of the references to colour in this figure legend, the reader is referred to the web version of this article.)

km/s) [37].

The longitudinal spin waves phase velocities dependencies on their wave vectors, obtained from the data in Fig. 12, are plotted in Fig. 13. The obtained phase velocities take maximum values (47 km/s) for H_{dc} = 150 Oe and wave vectors of the order of 0.7 μm^{-1}. Conversely, the slower phase velocities (9 km/s) are associated to the lower dc fields (30 Oe) and the larger wave vectors (4.4 μm^{-1}). The obtained phase velocity for H_{dc} = 40 Oe and at a 4.0 GHz H_{rf} field (k = 1.1 μm^{-1}) is in complete agreement with the value obtained from the data in Fig. 10 (22 km/s).

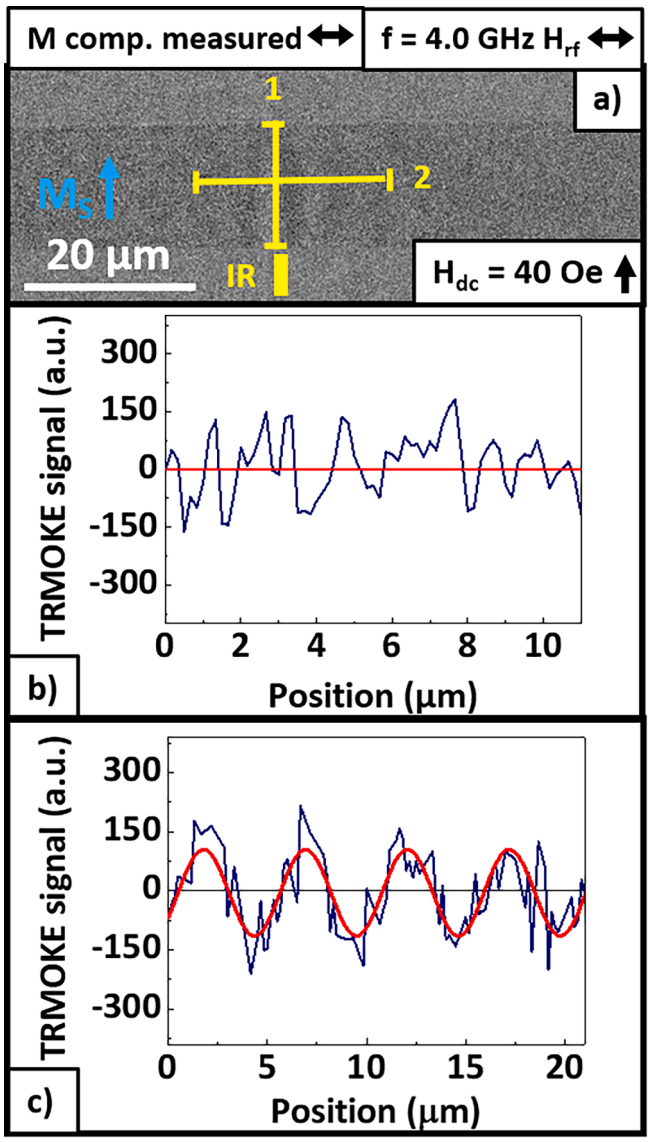

Fig. 9. a) TRMOKE image taken in the the AM zone by applying the fields and implementing the measuring configurations indicated (the measured local orientation of the dc magnetization is indicated by the blue arrow), b) Position dependence of the instantaneous TRMOKE signal measured along line 1 in a) (zero position corresponds to the most upward point in line 1), and c) Position dependence of the instantaneous TRMOKE signal measured along line 2 in a) (zero position corresponds to the most leftward point in line 2). The red line in c) corresponds to the fit of the data to a sinusoidal function. (For interpretation of the references to colour in this figure legend, the reader is referred to the web version of this article.)

Our data for the frequency dependence of the effective propagation distance of the spin waves excited at the IR by using different H_{rf} field frequencies and under transverse H_{dc} fields with different magnitudes are displayed in Fig. 14. The data in this plot have been obtained from fits of the spatial variation of the local TRMOKE signal amplitude of the type shown in Fig. 11 (i.e.: fits to the H_{rf} field frequency sinusoids with exponentially decaying amplitudes). In particular, the considered spin waves amplitude decay considered when evaluating the propagation distance, corresponds to 90% of the amplitude at the IR. From Fig. 14, the propagation distance increases with the increase of the magnitude of the applied dc field and with the decrease of the H_{rf} field frequency, reaching in our data set maximum values of the order of 41 μm.

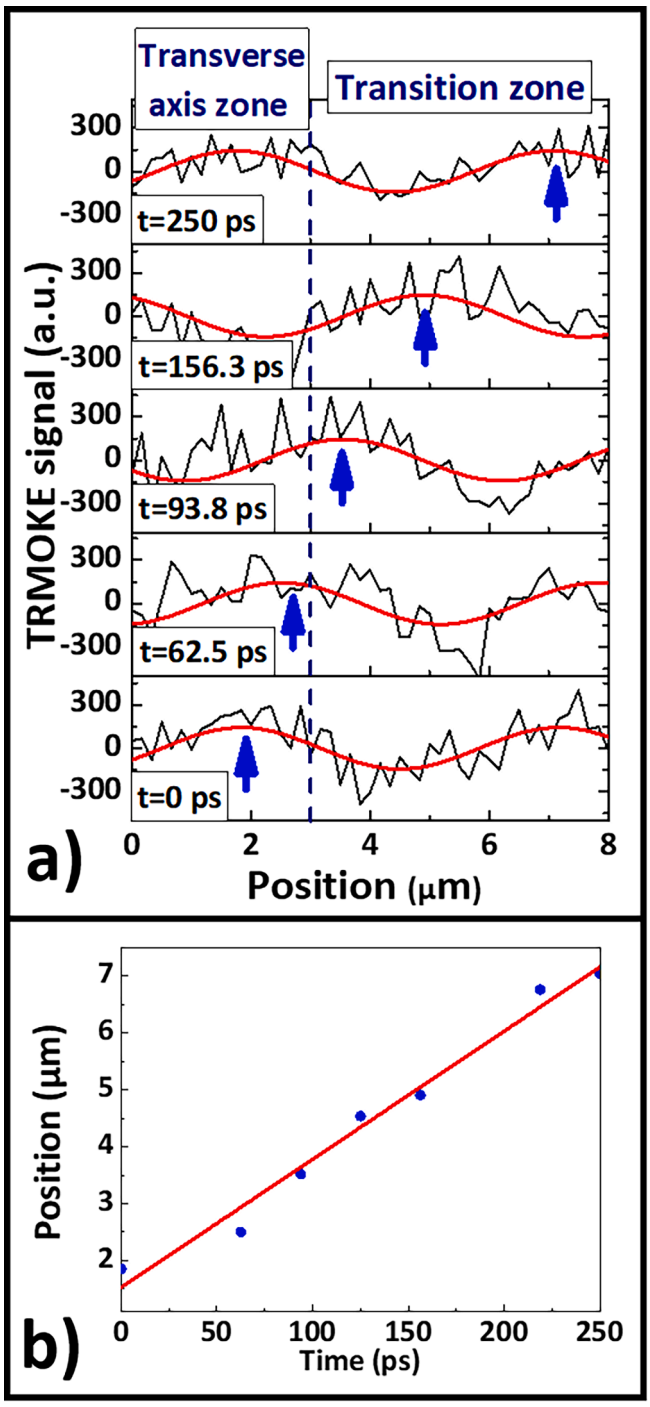

Fig. 10. a) Spatial variation of the instantaneous TRMOKE signal, measured at points in the range from the IR center (zero position) to 8 μm rightwards from that point (the limit between the IR and the transition region is shown), for different times after an arbitrary zero reference (4 GHz H_{rf} field frequency). b) Displacement of the instantaneous TRMOKE signal maximum marked with the blue arrow in a) as a function of time (see text for additional data on the excitation of the propagating spin waves). (For interpretation of the references to colour in this figure legend, the reader is referred to the web version of this article.)

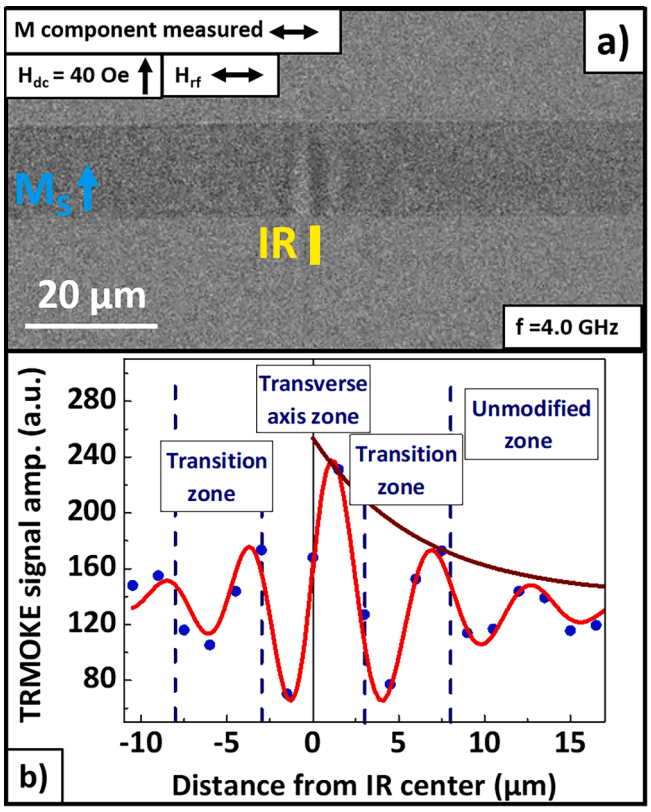

Fig. 11. a) Longitudinal spin waves excited by means of the fields configuration detailed and imaged by using the identified measuring parameter (the measured local orientation of the dc magnetization is indicated by the blue arrow). b) Spatial variation, around the IR center, of the local TRMOKE signal amplitude and its fit to a sinusoid (red line) whose amplitude decays exponentially from the center of the IR (brown line). The limits between the different anisotropy zones are shown. (For interpretation of the references to colour in this figure legend, the reader is referred to the web version of this article.)

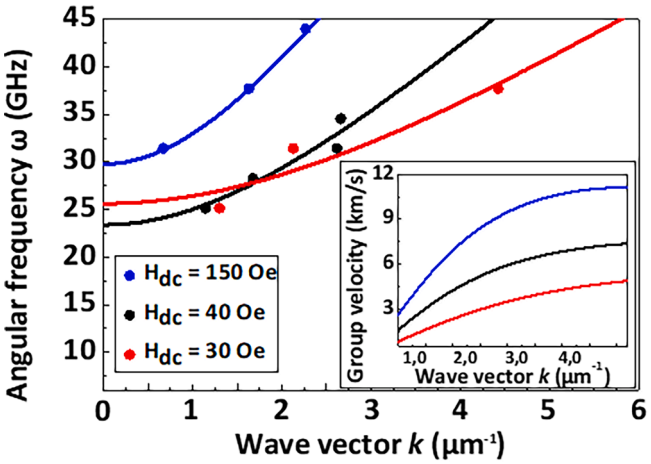

Fig. 12. Dispersion relationships verified by the longitudinal spin waves propagating at the AM zone under different transverse applied dc fields (the lines are fits to equation (1)). The inset shows the plot of the longitudinal spin waves group velocity dependence on their wave vector.

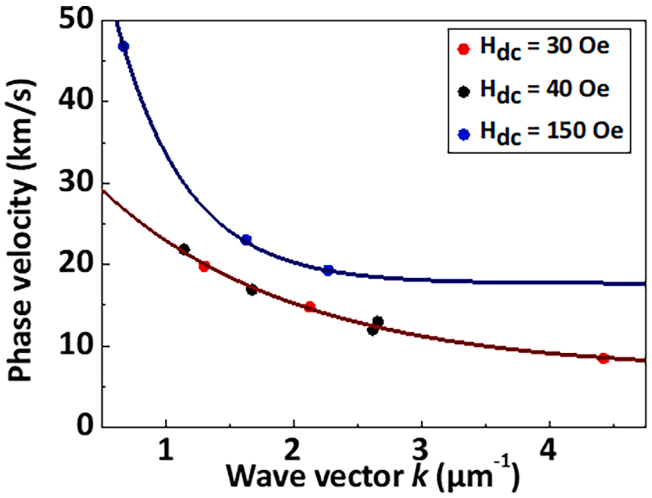

Fig. 13. Wave vector dependencies of the phase velocities corresponding to the longitudinal spin waves excited at the AM zone for different applied dc fields. (the lines are a guide for the eye and a single line is used for the data corresponding to 30 and 40 Oe applied dc fields).

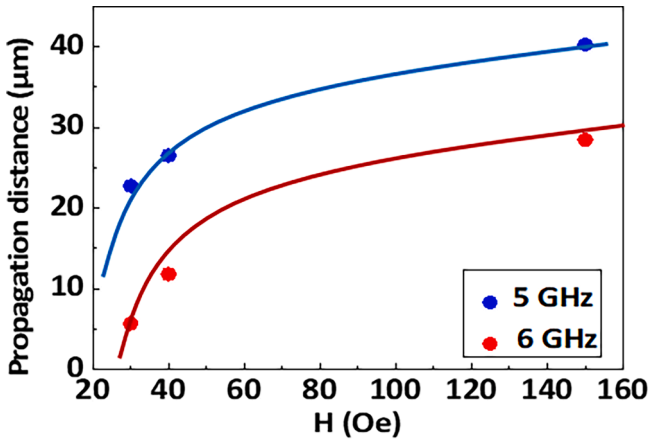

Fig. 15. Transverse applied dc field dependencies of the longitudinal spin waves effective propagation distances for 5 GHz and 6 GHz H_{rf} field frequencies. The lines are guides for the eye. Regarding the damping behavior of the longitudinal spin waves propagating at the AM zone, Fig. 16 displays the frequency and applied dc field variation of the corresponding effective coefficient, α, evaluated considering the equation [38]:

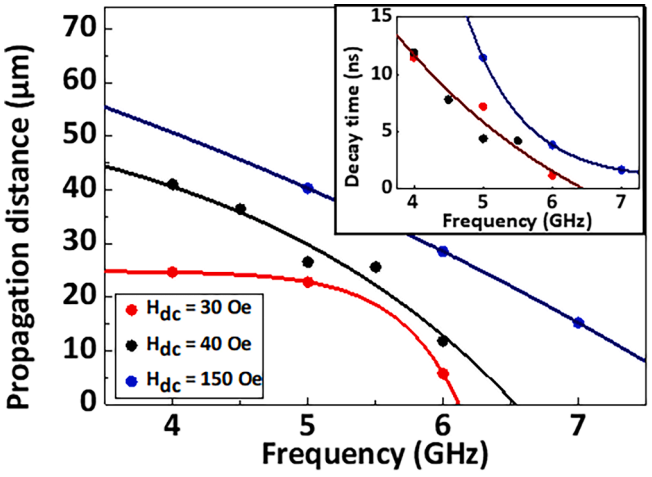

Fig. 14. Frequency dependence of the longitudinal spin waves effective propagation distances corresponding to different H_{dc} fields (evaluated from the exponential decay of the spatial dependence of spin waves amplitudes). The inset shows the frequency dependence of the spin waves decay time.

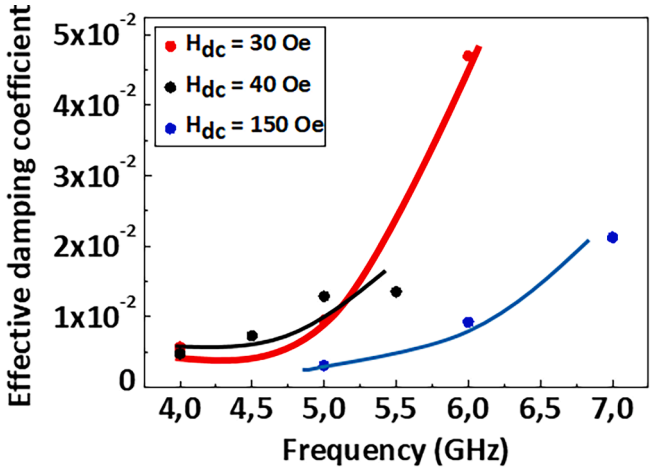

Fig. 16. H_{rf} field frequency and applied dc field dependencies of the effective spin waves damping constant evaluated from the propagation distances measured for the propagating spin waves excited at the AM zone .

Consistently with the data obtained in the case of the transverse standing waves excited at 7.5 GHz under a dc field of 250 Oe, the value of the propagation distance obtained here, at 7 GHz under 150 Oe is of 17 μm, which evidences the isotropy of the attenuation process taking place in the stripes. It is clear that in our case, the longitudinal spin waves propagation is constrained by the longitudinal dimension on the X-ray induced AM region, which the authors estimated in a previous work on 16 μm [21]. The inset in Fig. 14 shows the frequency dependence of the decay time linked to the propagation time through the spin waves group velocities. The maximum decay time values are obtained for the smaller applied dc fields and the smaller H_{rf} fields frequencies.

The effective propagation distance values obtained for 5 and 6 GHz and different applied dc fields are plotted in Fig. 15 That propagation distance, increasing with the applied field, takes maximum values (ca. 40 μm) at 150 Oe and a H_{rf} frequency of 5 GHz. The minimum measured propagation distance (6 μm) was obtained for 30 Oe at 6 GHz. These propagation distances, are comparable to others obtained in magnonic applications thin film candidate materials such as YIG (60 μm) [34], Permalloy (40 μm) [35], YIG-Pt bilayers (31 μm) [36] and CoMnFeSi (16.7 μm) [38].

$$\alpha = \frac{1}{2\pi\tau_0 f_0} \tag{2}$$

where τ_0 is the spin wave decay time shown on the inset in Figure 14 and f_0 is the frequency of the uniform precession (k = 0) associated to each H_{dc} applied field value. The latter data was obtained from a previous work by the authors [21] (f_0 (30 Oe) = 2.32 GHz; f_0 (40 Oe) = 2.80 GHz; f_0 (150 Oe) = 4.49 GHz). The effective damping increases with the H_{rf} frequency for all the applied dc fields, taking values from 3.1×10^{-3} (150 Oe, 5.0 GHz) to 4.7×10^{-2} (30 Oe, 6.0 GHz). The lowest measured values agree, independently from the applied field, with those obtained from FMR measurements on $Fe_{80}B_{20}$ amorphous thin films deposited onto MgO (0 0 1) ($\alpha = 4.0 \times 10^{-3}$) and Corning® glass ($\alpha = 3.5 \times 10^{-3}$) [26]. These values are also comparable to others directly measured by SW imaging on Permalloy ($\alpha = 6.5 \times 10^{-3}$) [35], CoFeB ($\alpha = 5.0 \times 10^{-3}$) [36] or CoMnFeSi ($\alpha = 3.0 \times 10^{-3}$) [38]. The obtained effective damping coefficient value furtherly qualifies amorphous $Fe_{80}B_{20}$ films as

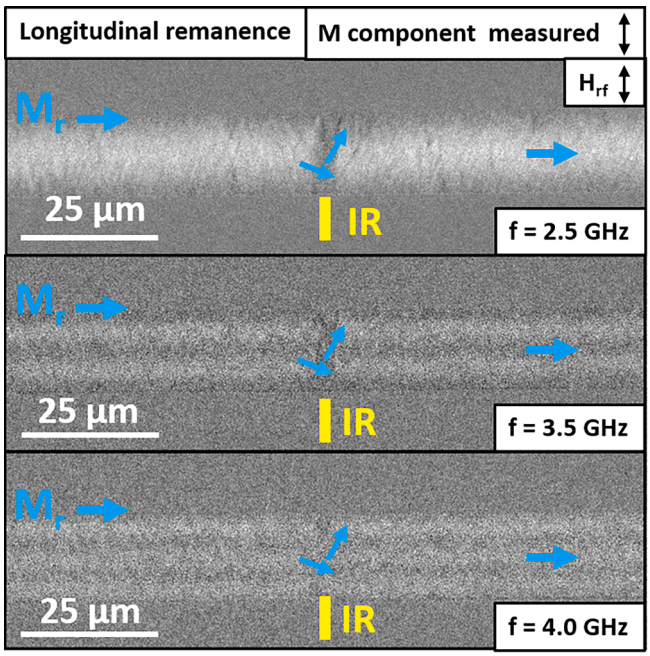

Fig. 17. TRMOKE images (transverse component of the magnetization measured) of the region around the IR obtained at the longitudinal remanence and under transverse H_{rf} fields having frequencies of a) 2.5 GHz, b) 3.5 GHz and c) 4.0 GHz. The measured local longitudinal component of the dc magnetization is indicated (at the irradiated and non-irradiated regions) by the blue arrows. (For interpretation of the references to colour in this figure legend, the reader is referred to the web version of this article.)

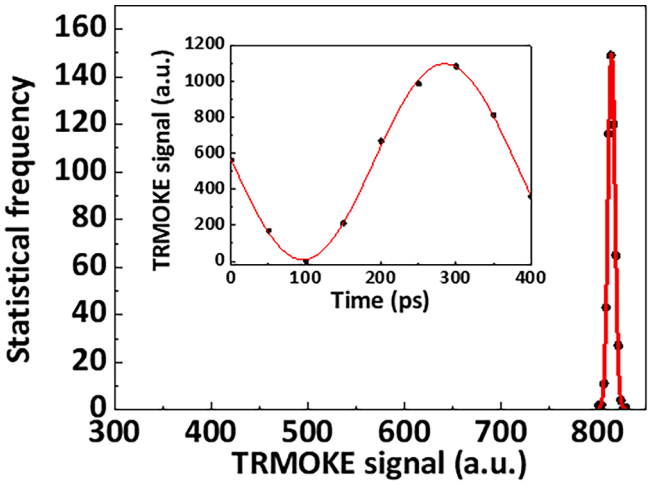

Fig. 18. Local TRMOKE signal magnitude distribution obtained at a 2 μm × 9 μm region within the IR (longitudinal saturation remanence, 2.5 GHz Hrf frequency). The inset shows the time evolution of the TRMOKE signal averaged over the whole IR.

candidate materials for magnonic devices implementations, since we have checked that it can transferred from thin films [26] to spin waves guides.

Considering now the interaction between the non-irradiated zones across the IR, it corresponds to clearly different behaviors depending on the relative orientation of the H_{rf} and H_{dc} fields with respect to the local, transverse, anisotropy at the IR. In the case corresponding to H_{rf} parallel to the IR transverse axis, the images shown in Fig. 17 (SB15 sample), corresponding to the longitudinal remanence and taken under transverse H_{rf} fields with frequencies of 2.5, 3.5 and 4.0 GHz, evidence the excitation at the non-irradiated regions of different standing transverse spin waves modes (indistinguishable from those shown in Fig. 5 and observed far from the IR). Those spin waves are even excited within the transition anisotropy zone, which could be explained as related to a) the exchange between the moments present at the transition region with those at the non-irradiated zone and b) the close-to-zero anisotropy values found at that transition zone [21]). Differently from the non-irradiated region behavior, the dynamics at the IR corresponds to a to a local, uniform, forced (non-resonant) precession of the magnetization around the effective field direction. The spatial uniformity of the precession is evidenced in Fig. 18 where we have plotted the instantaneous statistical distribution of the TRMOKE signal values (considered within a 2 μm × 9 μm region centered at the IR center), evaluated at the longitudinal remanence and under a 2.5 GHz H_{rf} field. That distribution exhibits an average value that is a ca. 40 times larger than the measured distribution width. The inset in Fig. 18 shows the time dependence of the instantaneous TRMOKE signal averaged over the whole IR. The maximum measured TRMOKE signal is of the order of a 60% of the resonance amplitude associated to 2 GHz [22]. The same processional behavior was observed at other H_{rf} frequencies (below 4 GHz). The observed uniform precession at the IR results from the local direction at that region of the dc magnetization exhibiting a component perpendicular to the H_{rf} field significantly lower than the saturation magnetization (see Fig. 2) [21,26].

When considering the non-irradiated zones coupling across the IR associated to the transverse dc remanence and H_{rf} perpendicular to the IR easy axis, it is possible to observe, Fig. 19 a), the occurrence of a phase shift between the transverse standing waves excited at both sides of the IR (H_{rf} field frequency of 4.0 GHz, M component measured parallel to the H_{rf} field). The same phase shift is observed, as shown in Fig. 19 b), for the magnetization component perpendicular to the H_{rf} field, which allows to identify the contrast as related to the polar Kerr effect [24] (out-of-plane component of the magnetization). The plots in Fig. 19 c) and d) (giving the position dependence of the TRMOKE signal along lines 1 and 2 in Fig. 19 a)) evidence that the magnitude of the observed phase shift corresponds to 176° ± 10°. In the particular case of the stripe measured in Fig. 19 a) to d) (SB15 sample) it was possible to observe at the remanence (Fig. 19 e)) a dc domain structure including the presence (similarly to Fig. 2 e)) of walls running parallel to the stripe axis (whereas the dc field was applied transversely in this image, the longitudinal component of the magnetization was measured). Taking into account the nature of broadband emitters of these domain walls [39], the observed phase shift would be the result of the convolution of the emissions of spin waves at the stripe edges, and the walls present at the transverse remanence and pinned at the IR.

4. Conclusions

The irradiation by means of synchrotron X-ray light of our lithographed amorphous $Fe_{80}B_{20}$ stripes results on the induction of a local anisotropy characterized by a transverse easy axis that stabilizes a 180° domain wall at the IR (in addition to side regions providing transition to the local anisotropy of the non-irradiated zone). At the non-irradiated region, we have identified the excitation of standing transverse spin waves whose dispersion relationships have been measured and fitted to a dipole-exchange model [32]. Those fits give values for the exchange correlation length coincident with the data in the literature, but do not provide adequate film thickness values. This is understood as a consequence of the fact that the wave vectors corresponding to our measurements fall in the boundary region between those associated to spin waves incorporating significant contributions from the exchange interactions and that corresponding to the pure magnetostatic spin waves. The group velocities obtained from the dispersion relationships range

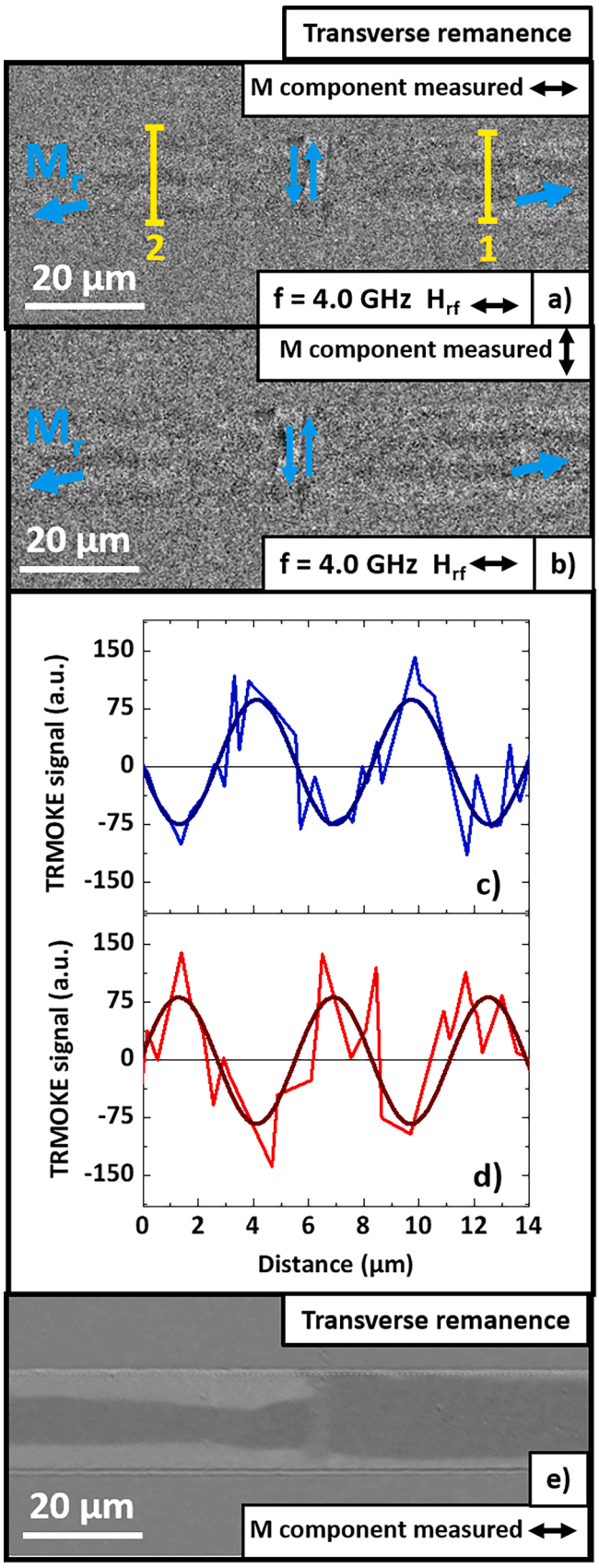

(caption on next column)

Fig. 19. a) TRMOKE image (M component measured parallel to H_{rf}) of the zone around the IR taken at the transverse remanence and under a H_{rf} field having a frequency of 4 GHz (the measured local orientation of the dc magnetization is indicated by the blue arrows); b) TRMOKE image (M component measured perpendicular to H_{rf}) of the zone around the IR taken at the transverse remanence and under a H_{rf} field having a frequency of 4 GHz (the measured local orientation of the dc magnetization is indicated by the blue arrows); c) Position dependence of the instantaneous TRMOKE signal measured along line 1 (in a)) and sinusoidal fit (in dark blue line); d) Position dependence of the instantaneous TRMOKE signal measured along line 2 (in a)) and sinusoidal fit (in dark red line). In both plots the zero position corresponds to the most upwards point in the lines along which the signal profiles have been measured; e) dc domain structure associated to the dynamic images. (For interpretation of the references to colour in this figure legend, the reader is referred to the web version of this article.)

from 1 km/s (longitudinal remanence H_{rf} field frequency of 2.5 GHz) up to 16 km/s (longitudinal field of $H_{dc} = 250$ Oe, H_{rf} field frequency of 7.5 GHz).

The presence of a differentiated local anisotropy at the IR is associated to a specific dynamic behavior that is observable as corresponding to the excitation of propagating longitudinal spin waves that are emitted at the center of the IR and whose amplitude gets negligible at distances from the emitting zone of the order of 40 μm. The experimental dispersion relationships of these longitudinal spin waves have also been fitted by considering a dipole-exchange model [31] that allow to evaluate group velocities in the range from 2 km/s (transverse $H_{dc} = 30$ Oe, wave vectors below 1 μm^{-1}) up to 9 km/s (transverse $H_{dc} = 150$ Oe, wave vectors above 4 μm^{-1}).

Interestingly, the interaction between the dynamic behavior of the non-irradiated zones and that of the IR corresponds, for H_{rf} field parallel to the IR easy axis and a longitudinal dc remanence, to a local uniform precession at the IR that is independent from the standing spin waves excited at the non-irradiated zone. Furthermore, for a H_{rf} field perpendicular to the transverse easy axis and a stripe transverse dc remanence, a phase shift of 180° between the out-of-plane transverse standing spin waves excited at both sides of the IR is found. This phase shift, taking place without any applied dc field, and being associated to the local anisotropy modification induced by the X-ray irradiation, opens the door to the use of our local anisotropy modification into the implementation of spin wave devices of the interferometric logic gate type.

CRediT authorship contribution statement

Unai Urdiroz: Investigation, Writing - review & editing. **Cai Müller:** Writing - review & editing. **Alicia Gómez:** Investigation. **M. Teresa Magaz:** Resources. **Daniel Granados:** Resources. **Marta Sánchez Agudo:** Investigation. **Juan Rubio-Zuazo:** Resources. **Germán R. Castro:** Resources. **Camelia Stan:** Resources. **Nobumichi Tamura:** Resources. **Howard A. Padmore:** Resources. **Federico Cebollada:** Conceptualization, Investigation, Writing - review & editing. **F. Javier Palomares:** Conceptualization, Investigation. **Jeffrey McCord:** Investigation, Writing - review & editing. **Jesús M. González:** Conceptualization, Writing - original draft, Writing - review & editing, Supervision.

Declaration of Competing Interest

The authors declare that they have no known competing financial interests or personal relationships that could have appeared to influence the work reported in this paper.

Acknowledgements

This work has been developed with funds corresponding to project MAT2016-80394-R financed by the Spanish Research Agency (AEI) and 2019AEP150 by A.E. Consejo Superior de Investigaciones Científicas (CSIC). We also acknowledge the Spanish Ministerio de Ciencia e Innovación and Consejo Superior de Investigaciones Científicas for financial support and for provision of synchrotron radiation at beamline BM25-SpLine (ESRF). A.G. acknowledges IJCI-2017-33991. U.U. acknowledges FPI grant BES-2014-070387. This research used resources of the Advanced Light Source, a DOE Office of Science User Facility under contract no. DE-AC02-05CH11231. J.M. and C.M. acknowledge funding from the German Research Foundation through grant DFG9/10-2.

Data availability.

The data that support the findings of this study are available from the corresponding author, [JMG], upon reasonable request.

References

[1] F. Bloch, Zur theorie des ferromagnetismus, Zeitschrift für Physik 61 (3–4) (1930) 206–219.
[2] C. Herring, C. Kittel, On the theory of spin waves in ferromagnetic media, Phys. Rev. 81 (5) (1951) 869.
[3] 3.Akhiezer, A. I.; Peletminskii, S.; Baryakhtar, V. G., Spin waves. 1968.
[4] E. Samuelsen, M. Hutchings, G. Shirane, Inelastic neutron scattering investigation of spin waves and magnetic interactions in Cr2O3, Physica 48 (1) (1970) 13–42.
[5] P. Fleury, S. Porto, L. Cheesman, H. Guggenheim, Light Scattering by Spin Waves in Fe F2, Phys. Rev. Lett. 17 (2) (1966) 84.
[6] F.J. Dos Santos, M. dos Santos Dias, F.S.M. Guimarães, J. Bouaziz, S. Lounis, Spin-resolved inelastic electron scattering by spin waves in noncollinear magnets, Phys. Rev. B 97 (2) (2018).
[7] S.Y. An, P. Krivosik, M.A. Kraemer, H.M. Olson, A.V. Nazarov, C.E. Patton, High power ferromagnetic resonance and spin wave instability processes in Permalloy thin films, J. Appl. Phys. 96 (3) (2004) 1572–1580.
[8] K. Zakeri, J. Lindner, I. Barsukov, R. Meckenstock, M. Farle, U. Von Hörsten, H. Wende, W. Keune, J. Rocker, S. Kalarickal, Spin dynamics in ferromagnets: Gilbert damping and two-magnon scattering, Phys. Rev. B 76, (10) 2007, 104416.
[9] D.L. Mills, S.M. Rezende, Spin damping in ultrathin magnetic films. In Spin Dynamics in Confined Magnetic Structures II, Springer (2003) 27–59.
[10] A. Serga, A. Chumak, B. Hillebrands, YIG magnonics, J. Phys. D Appl. Phys. 43 (26) (2010).
[11] P. Malago, L. Giovannini, R. Zivieri, P. Gruszecki, M. Krawczyk, Spin-wave dynamics in permalloy/cobalt magnonic crystals in the presence of a nonmagnetic spacer, Phys. Rev. B 92 (6) (2015).
[12] P. Fischer, H. Ohldag, X-rays and magnetism, Rep. Prog. Phys. 78 (9) (2015).
[13] C. Back, J. Heidmann, J. McCord, Time resolved Kerr microscopy: Magnetization dynamics in thin film write heads, IEEE Trans. Magn. 35 (2) (1999) 637–642.
[14] T. Sebastian, K. Schultheiss, B. Obry, B. Hillebrands, H. Schultheiss, Micro-focused Brillouin light scattering: imaging spin waves at the nanoscale, Front. Phys. 3 (2015) 35.
[15] A. Khitun, M. Bao, K.L. Wang, Magnonic logic circuits, J. Phys. D Appl. Phys. 43 (26) (2010).
[16] S.A. Nikitov, D.V. Kalyabin, I.V. Lisenkov, A. Slavin, Y.N. Barabanenkov, S.A. Osokin, A.V. Sadovnikov, E.N. Beginin, M.A. Morozova, Y.A. Filimonov, Magnonics: a new research area in spintronics and spin wave electronics, Physics-Uspekhi, 58, (10), 2015, 1002.
[17] A.V. Chumak, V.I. Vasyuchka, A.A. Serga, B. Hillebrands, Magnon spintronics, Nat. Phys. 11 (6) (2015) 453–461.
[18] K.-S. Lee, S.-K. Kim, Conceptual design of spin wave logic gates based on a Mach–Zehnder-type spin wave interferometer for universal logic functions, J. Appl. Phys. 104 (5) (2008).
[19] O.V. Dobrovolskiy R. Sachser S.A. Bunyaev D. Navas V.M. Bevz M. Zelent, W. Śmigaj, J. Rychły, M. Krawczyk, R.V. Vovk, Spin-wave phase inverter upon a single nanodefect. ACS App. Mater. Interf. 11, (19) 2019, 17654-17662.
[20] R. Hertel, W. Wulfhekel, J. Kirschner, Domain-wall induced phase shifts in spin waves, Phys. Rev. Lett. 93 (25) (2004).
[21] U. Urdiroz, A. Gómez, M. Magaz, D. Granados, M.S. Agudo, J. Rubio-Zuazo, G. Castro, C. Stan, N. Tamura, H. Padmore, C. Müller, J. McCord, F. Cebollada, F.J. Palomares, J.M. González, Antiphase resonance at x-ray irradiated microregions in amorphous Fe80B20 stripes, J. Magnet. Magnet. Mater. 167017, 2020.
[22] M. Kunz, N. Tamura, K. Chen, A.A. MacDowell, R.S. Celestre, M.M. Church, S. Fakra, E.E. Domning, J.M. Glossinger, J.L. Kirschman, A dedicated superbend X-ray microdiffraction beamline for materials, geo-, and environmental sciences at the advanced light source, Rev. Sci. Instrum. 80 (3) (2009).
[23] J. McCord, Progress in magnetic domain observation by advanced magneto-optical microscopy, J. Phys. D Appl. Phys. 48 (33) (2015).
[24] R.B. Holländer, C. Müller, M. Lohmann, B. Mozooni, J. McCord, Component selection in time-resolved magneto-optical wide-field imaging for the investigation of magnetic microstructures, J. Magn. Magn. Mater. 432 (2017) 283–290.
[25] B. Mozooni, T. von Hofe, J. McCord, Picosecond wide-field magneto-optical imaging of magnetization dynamics of amorphous film elements, Phys. Rev. B 90 (5) (2014).
[26] U. Urdiroz, B. Teixeira, F. Palomares, J. Gonzalez, N. Sobolev, F. Cebollada, A. Mayoral, Dynamic magnetic properties of amorphous Fe80B20 thin films and their relation to interfaces, AIP Adv. 10 (1) (2020).
[27] Urdiroz U., Palomares F.J., Mayoral A., Soldatov I.V., Schäfer R., Gonzalez J.M., Sánchez Agudo M., Navarro E., Ruiz A., Alonso M., Vázquez L., and Cebollada F Role of the interfaces in the crystallization and hysteresis mechanisms of amorphous Fe-B thin films, J.Alloys Comp. 869, 2021, 159276–1/12.
[28] M. Lohman, B. Mozooni, J. McCord, Homogeneous microwave field emitted propagating spin waves: Direct imaging and modeling, J. Magn. Magn. Mater. 450 (2018) 7–12.
[29] C. Davies, V. Poimanov, V. Kruglyak, Mapping the magnonic landscape in patterned magnetic structures, Physical Review B 96 (9) (2017).
[30] J. Adam, T. O'Keeffe, R. Patterson, Magnetostatic wave to exchange resonance coupling, J. Appl. Phys. 50 (B3) (1979) 2446–2448.
[31] S. Tacchi, R. Silvani, G. Carlotti, M. Marangolo, M. Eddrief, A. Rettori, M.G. Pini, Strongly hybridized dipole-exchange spin waves in thin Fe-N ferromagnetic films, Physical Review B 100 (10) (2019).
[32] https://physics.nist.gov/cgi-bin/cuu/Value?gammaebar.
[34] C. Liu, Chen J. Liu T., Heimbach, F., Yu, H., Xiao, Y., Hu, J., Liu, M., Chang, H., Stueckler, T., Long-distance propagation of short-wavelength spin waves, Nat. Commun. 9 (1), 2018 1-8.
[35] M. Bailleul, D. Olligs, C. Fermon, S. Demokritov, Spin waves propagation and confinement in conducting films at the micrometer scale, EPL (Europhysics Letters) 56 (5) (2001) 741.
[36] H. Yu, O. d'Allivy Kelly, V. Cros, R. Bernard, P. Bortolotti, A. Anane, F. Brandl, R. Huber, I. Stasinopoulos, D. Grundler, Magnetic thin-film insulator with ultra-low spin wave damping for coherent nanomagnonics, Sci. Rep. 4 (2014) 6848.
[37] P. Pirro, T. Brächer, A. Chumak, B. Lägel, C. Dubs, O. Surzhenko, P. Görnert, B. Leven, B. Hillebrands, Spin-wave excitation and propagation in microstructured waveguides of yttrium iron garnet/Pt bilayers, Appl. Phys. Lett. 104 (1) (2014).
[38] T. Sebastian, Y. Ohdaira, T. Kubota, P. Pirro, T. Brächer, K. Vogt, A. Serga, H. Naganuma, M. Oogane, Y. Ando, Low-damping spin-wave propagation in a micro-structured Co2Mn0.6Fe0.4Si Heusler waveguide, Appl. Phys. Lett. 100 (11) (2012).
[39] R.B. Holländer, C. Müller, J. Schmalz, M. Gerken, J. McCord, Magnetic domain walls as broadband spin wave and elastic magnetisation wave emitters, Scient. Rep. 8 (1) 2018 13871 1–11.